Aeolian erosion thresholds for cohesive sand

Jean-Baptiste Besnard, Pascal Dupont, Ahmed Ould El Moctar, Alexandre Valance

Aeolian erosion thresholds for cohesive sand

J-B. Besnard[1,2], P. Dupont[2], A. Ould El Moctar[3], A. Valance[1]

[1]Univ Rennes, CNRS, Institut de Physique de Rennes, UMR 6251, 35 042 Rennes, France
[2]Univ Rennes, INSA Rennes, LGCGM, 35 043 Rennes, France
[3]Univ Nantes, CNRS, Laboratoire Thermique et Energie, UMR 6607, 44306 Nantes Cedex, France

Key Points:

- We devised a new approach to assess the aerodynamic and dynamic transport thresholds for cohesive sand beds in wind-tunnel experiments.
- The aerodynamic threshold is found to increase linearly with the amount of liquid content within the sand bed.
- Unlike the aerodynamic threshold, the dynamic threshold remains unchanged in the range of cohesive strength investigated so far.

Corresponding author: A. Valance, alexandre.valance@univ-rennes1.fr

Abstract

Moisture is known to affect sand cohesion and therefore transport threshold and rate of aeolian sand transport. Aeolian sand transport has been widely documented for dry sand beds, but much more sparsely in the context of moist sand beds. One major challenge in the collection of reliable field or laboratory data for moist sand is to have an accurate control of the moisture level within the sand bed, which is prone to strongly vary over time and space due to evaporation. To suppress the variability of moisture content due to evaporation, we devised a new approach based on the use of a non-volatile liquid (namely silicon oil instead of water) which ensures a proper control of the liquid content. We thus conducted wind-tunnel experiments employing this approach and observed that the aerodynamic threshold friction velocity increases linearly with liquid content, while the dynamic threshold is found to be unchanged in the range of cohesion strength investigated in this study. These outcomes indicate that the difference between the static and dynamic threshold increases with increasing cohesion. This may have strong implications on aeolian transport of moist sand, and in particular on hysteretic behaviors.

Plain Language Summary

Moisture has a significant influence on the initiation of motion of sand by wind and also on the resulting sand transport rate. While the moisture level is usually very low in sandy desert areas and thus irrelevant there, the aeolian sand transport on sandy beaches or in the context of coastal dune morphodynamics is expected to be crucially dependent on the moisture content within the sand. The literature regarding the impact of the moisture on wind blown sand is sparse, and available data exhibit considerable discrepancies regarding the magnitude of the moisture effects. These discrepancies highlight that it is experimentally difficult to control the moisture levels within the sand because of evaporation. To circumvent this difficulty, we carried wind-tunnel experiments with sand-oil mixtures instead of sand-water mixtures. Oil plays the same role as water in generating cohesion but has the significant advantage to have a very low evaporation rate in the standard conditions of temperature and pressure. With these sand-oil mixtures, we were able to assess with an unprecedented accuracy the magnitude of the cohesion effects on the aerodynamic erosion threshold and also on the threshold characterizing the cessation of transport, known as the dynamic threshold.

1 Introduction

Aeolian processes that involve the entrainment, transport, and deposition of sediment by the wind are important geomorphic processes operating in arid regions but also along sandy shores. They are responsible in particular for the formation and migration of sand dunes. Understanding these processes in complex environments (e.g., in the presence of vegetation or in the context of cohesive soils) demands further investigations.

Wind blown sand involves a myriad of physical mechanisms, including particle-particle, bed-particle and fluid-particle interactions. A comprehensive quantification of these interactions in the context of cohesive particulate beds remains a scientific challenge. Aeolian sand transport with non-cohesive particles can be regarded as one of the simplest air-particulate flows, while the transport of moist sand or snow exhibits a much greater complexity.

The complexity of the aforementioned real cohesive systems arises from the fact that the strength of the cohesion may strongly evolve in time and space. Monitoring these variations in situ at the relevant temporal and spatial scales is beyond of the classical instrumental capabilities. Promising instruments based on capacitance measurements (Louge et al., 2010, 2013, 2022) are however, capable of monitoring tiny variations of moisture content at the surface of a sand bed and within the bed with a centimetric spatial resolution and should be further deployed on the field or in wind tunnel experiments to better document the coupling between sand transport and cohesion. This capacitance technique has already proven to be effective to probe the temporal evolution of the water content within a barchan dune (Louge et al., 2013,

2022). Also, the potential effects of inter-particle cohesion on the transfer of mass, momentum and energy between the moving particles and the static bed remain poorly documented (Namikas & Sherman, 1995). Thus, predicting mass transport rates for these complex systems is very uncertain.

An important issue in wind-blown sand concerns the critical air flow velocity at which transport starts and ceases. These thresholds are referred to as the aerodynamic and dynamic thresholds, respectively (Bagnold, 1941; Kok & Rennó, 2009; Duran et al., 2011; Valance et al., 2015; Pähtz et al., 2020). Different physical interpretations of the dynamic threshold can be found in the literature. Some authors (Pähtz et al., 2020, 2021) interpret the latter as the rebound threshold, describing the smallest wind friction velocity to sustain a continuous saltation motion of a single grain along the bed. This hypothesis is independent of the ejection process, but related to the properties of the rebound. Other ones (Duran et al., 2011; Jenkins & Valance, 2014; Valance et al., 2015) define the dynamic threshold to be the minimum wind speed to sustain a non-zero saturated flux. In the latter perspective (as detailed further below), the dynamic threshold is related to the splash process and the replacement capacity.

For dry aeolian sand of $200\,\mu m$ size, the dynamic threshold is significantly smaller (20% less (Bagnold, 1941; Ho, 2012)) than the aerodynamic one and this is due to the fact that once transport has been initiated, erosion induced by the impact of grains onto the bed is a very efficient mechanism to sustain the saltation transport (Beladjine et al., 2007; Creyssels et al., 2009). This hysteretic effect between initiation and cessation is expected to be drastically modified for cohesive beds as suggested by the recent numerical work from Comola, Gaume, et al. (2019) which showed in the context of snow transport that saltation over cohesive beds sustains itself at wind speeds 1 order of magnitude smaller than those necessary to initiate it. We shall also mention a recent experimental work in a closed-loop wind-tunnel by Andreotti et al. (2021) which questions the existence of two distinct thresholds. They did not observe any difference between the aerodynamic and dynamic thresholds when increasing or decreasing the wind strength and ascribe this outcome to the essential role of the turbulent flow velocity fluctuations, which are probably strongly enhanced by the closed-loop wind-tunnel.

Most of the studies dedicated to transport of moist sand focused on the modification of the aerodynamic threshold with the moisture level (Chepil, 1956; Belly, 1962; Bisal & Hsieh, 1966; Hotta et al., 1984; McKenna-Neuman & Nickling, 1989; Cornelis et al., 2004a; Han et al., 2009). The presence of moisture in sand is known to create cohesive forces between grains and has thus a strong influence on the initiation of sand transport which requires higher wind strengths. The aerodynamic threshold, also referred to as the static threshold, is defined as the minimum wind friction velocity to set grains into motion from a resting situation (Bagnold, 1941). For a cohesionless sand bed, the transport is initiated when the friction velocity overpasses a critical value u_s^* given by

$$u_s^* = A\sqrt{\frac{(\rho_p - \rho_f)}{\rho_f} g D}\,, \tag{1}$$

where D is the mean grain diameter, ρ_p and ρ_f are the particle and fluid density, respectively, and A is an empirical coefficient of order of 0.1 (Bagnold, 1941). This relationship can be inferred from a simple force balance between the aerodynamic force and the weight exerted on a grain at the sand bed surface. A typical value of the aerodynamic threshold for dry sand obtained in wind-tunnel is $u_s^* = 0.21\ m/s$ for sand grains with a mean diameter $D = 0.2\ mm$ (Ho et al., 2011). It is worth mentioning that the aerodynamic threshold is experimentally difficult to assess because the latter is sensitive to additional parameters that are not easy to properly control or characterize, like the level of the turbulent fluctuations of the air flow or the disorder at the surface of the bed (Duran et al., 2011). As an example, Pähtz et al. (2018) emphasize that the thickness of the turbulent boundary layer plays an important role in the initiation of sand transport and consequently, the aerodynamic threshold measured in natural conditions is often smaller than that measured in wind-tunnel experiments.

For moist sand, the aerodynamic threshold is an increasing function of the water content, but the literature presents a wide spectrum of results regarding the magnitude of moisture effects on the aerodynamic threshold. From wind-tunnel experiments with 0.44 *mm* sand grains, Belly (1962) reported a logarithmic evolution of the static threshold friction velocity with the water content ω (expressed in percent) from $\omega \approx 0.046\%$ to $\omega = 4\%$:

$$u^*_{sw} = u^*_s \, (1.8 + 0.6 \, \log \, \omega) \ . \tag{2}$$

In contrast, Hotta et al. (1984) proposed a linear relationship also on the basis of wind-tunnel experiments which is verified up to $\omega = 8\%$:

$$u^*_{sw} = u^*_s \, (1 + a_H \, \omega) \ . \tag{3}$$

The authors found that the slope a_H decreases with increasing grain diameter D: $a_H \approx 0.94, 0.30$ and 0.22 for $D = 0.2, 0.5$ and 0.8 *mm*, respectively. As highlighted by Hotta et al. (1984), the great diversity in the experimental data regarding the effect of the moisture on the aerodynamic threshold illustrates the difficulty of controlling the moisture levels within the bed due to evaporation. To mitigate the evaporation process, some of the wind-tunnel experiments were conducted with a saturated air flow, as done by Belly (1962), McKenna-Neuman and Nickling (1989) and V. J.-L. Ralaiarisoa (2020). However, it is quite difficult to maintain an air flow at saturation (i.e., $RH = 100\%$). As a consequence, the water content of the sand bed and in particular within the first layers of the surface is rapidly varying in space and time either through evaporation (under-saturated air) or condensation (over-saturated air), resulting in an erroneous estimation of the actual water content of the sand surface at the precise instant when sand transport is triggered. Recent experiments (V. J.-L. Ralaiarisoa, 2020) reported an intermittent transport regime completely controlled by cyclic evaporation of the superficial layers of the sand bed.

Some theoretical models were developed to predict the modification of the static threshold due to cohesion. McKenna-Neuman and Nickling (1989) derived an expression for the critical shear velocity using a force balance between the grain weight P_g, the cohesive force F_c and the wind shear stress:

$$u^*_{sw} = u^*_s \, \sqrt{1 + \alpha \, Co} \, , \tag{4}$$

where $Co = F_c / P_g$ is the dimensionless cohesion number and α is a constant geometrical parameter ($\alpha \approx 3$). This relationship is similar to that proposed by Shao and Lu (2000). To take benefit of the above relationship, the knowledge of the cohesive force F_c at the grain scale and its dependence on the water content is required, which is an experimental challenge with grains of submillimeter size. More elaborated expressions can be found in the literature (Cornelis et al., 2004b; Claudin & Andreotti, 2006). Eq. 4 is however useful to infer the strength of the cohesion from the assessment of the static threshold friction velocity u^*_{sw}.

The other important threshold in wind-blown sand is the dynamic threshold, also referred to as the impact threshold. According to Duran et al. (2011) and Valance et al. (2015), we define it as the minimal friction speed u^*_d for which a non-zero saturated flux can be sustained. A practical method to determine it is to extrapolate to zero the curve relating the sediment flux to the shear velocity (cf Eq. 5). It is thus defined in a much more accurate manner than the static threshold, for which a somewhat arbitrary criterion for the onset of particle motion has to be chosen. The key point explaining this dynamic threshold is the ability of grains in saltation to eject other grains, the so-called splash process (Kok & Rennó, 2009; Duran et al., 2011; Valance et al., 2015). This process is a statistical process, with a wide distribution of velocities and angles. In a steady state of transport, the distribution of grain velocities is stationary and on average, each saltating grain produces a single saltating grain after a collision with the bed, either by rebound or by ejection: the capture by the bed of low energy grains that have a probability to stop is balanced by the ejection of new grains by high energy impacts. One can formally define the replacement capacity as the average number of saltating grains produced per collision. At equilibrium, the replacement capacity is exactly 1. In this perspective, the dynamic threshold is crucially dependent on the splash process. The sand transport model

developed in (Creyssels et al., 2009) that incorporates explicitly the key features of the splash process indicates that the dynamic threshold is intimately linked to the critical impact velocity to trigger the ejection process. As mentioned previously, an alternative interpretation of the dynamic threshold based on the rebound threshold was proposed (Pähtz et al., 2020, 2021) and is still unclear which is the more relevant to describe the satured transport state at vanishing flux. The dynamic threshold is smaller than the static one and is about 80% of the latter (Bagnold, 1941; Ho, 2012) in the context of aeolian sand transport on earth with $200\,\mu m$ grain size.

The difference between the static and dynamic threshold is in particular crucially dependent on the grain to fluid density ratio as mentioned by Duran et al. (2011). This difference leads to bi-stability and hysteric behaviors when the wind friction velocity lies between the dynamic and static threshold (Martin & Kok, 2018; Comola, Kok, et al., 2019). Indeed, two stable states can coexist: a state with no transport and another one with a finite mass flux. The latter state can be only obtained with specific boundary or initial conditions (e.g, with a finite upwind mass flux or starting from a transport state with $u^* > u_s^*$ and decreasing the friction speed below u_s^*).

Importantly, the dynamic threshold is a key parameter of the transport law (Duran et al., 2011; Valance et al., 2015). The transport law quantifies the transport capacity of the turbulent air flow as a function of the wind shear stress in the equilibrium state, i.e., when erosion is exactly balanced by deposition. The mass flow rate at equilibrium is usually referred to as the equilibrium or saturated flux (Duran et al., 2011; Valance et al., 2015). For cohesionless sand beds, it scales linearly with the Shields number $S^* = \rho_f u^{*2}/(\rho_p - \rho_f)gD$ (Duran et al., 2011; Valance et al., 2015)

$$Q_{sat} = A_Q \rho_p D u_d^* \left(S^* - S_d^*\right) , \tag{5}$$

where S_d^* is the critical Shields numbers corresponding to the dynamic friction threshold u_d^* and A_Q is a numerical constant. This linear scaling holds in the saltation regime, but breaks down for very strong winds (i.e., $S^* > 10 S_d^*$) (J.-L. Ralaiarisoa et al., 2020).

Two important unresolved issues then arise: how the dynamic threshold is altered in the presence of cohesion and how the transport law is modified? In contrast to the static threshold, the modification of the dynamic threshold in the presence of cohesion has not received a lot of attention. There are very few studies on this issue. We are not aware of experimental studies aiming at determining the dynamic transport threshold as a function of the level of moisture. We can however mention two recent related numerical studies: the work by Comola, Gaume, et al. (2019) which investigates the splash process in the context of snow transport and the one by V. Ralaiarisoa et al. (2022) dedicated to the numerical study of the impact process on cohesive granular packings in the context of aeolian transport for moist sand. The main difference between these two studies is the nature of the cohesion. In the former one, the cohesion is ensured by solid (ice) bonds and the bond breakage is irreversible. In contrast, in the latter study, bonds are water capillary bridges and the breakage is reversible. One of the salient results in (V. Ralaiarisoa et al., 2022) is that the critical impact velocity to trigger the ejection process and its efficiency (i.e., the number of ejected particles per impact) are modified when the cohesion number exceeds a critical value of order 5. Numerical simulations from Comola, Gaume, et al. (2019) confirm that for high cohesion, the efficiency of the ejection process is substantially decreased. These numerical findings thus suggest that for strong cohesion, the dynamic transport threshold should be enhanced. Experimental evidences are however lacking. Concerning the modification of the equilibrium mass flux in the context of cohesive beds, there is no definite answer (McKenna-Neuman & Maljaars, 1998; Davidson-Arnott et al., 2008) due again to the difficulty to conduct experiments with an accurate control of the cohesion within the bed. The limit case corresponding to infinite cohesion (i.e., a rigid bed) is well documented. The experimental study from Ho et al. (2011) reported that the transport capacity over a rigid bed is much greater than over an equivalent erodible bed because the rebound is less dissipative. This was confirmed and explained through a simple two-phase transport model based on periodic trajectories (Jenkins & Valance, 2014). Consequently, as suggested by Davidson-Arnott et al. (2008), we may expect that for large cohesion strength, the saturated flux should

overpass the one corresponding to the cohesionless case. The numerical simulations from Comola, Gaume, et al. (2019) achieved in the context of snow transport provide some indications about the equilibrium mass flux for cohesive beds. Their results indicate that the equilibrium (i.e., saturated) mass flux increases with increasing but rather moderately: for very strong cohesion (i.e., $Co \approx 10^4$), the flux is found to increase only by a factor 1.25 in comparison with the cohesionless case.

The last important issue concerns the equilibrium length (resp. time) needed to reach the equilibrium state from a rest state. For the cohesionless case, several studies were devoted to this complex issue (Andreotti et al., 2010; Selmani et al., 2018). The general belief is that the equilibrium length increases with increasing the cohesion strength, but there are very few experimental quantitative studies on this question (Davidson-Arnott et al., 2008; V. J.-L. Ralaiarisoa, 2020). This belief was however confirmed recently by the numerical simulations from Comola, Gaume, et al. (2019). The increase of the equilibrium length with increasing cohesion can be explained by the lower efficiency of the splash process (i.e., production of ejected particles) with cohesive beds as argued by Comola, Gaume, et al. (2019).

We propose here an original experimental approach to determine both the static and dynamic threshold in the context of cohesive sand beds in an unprecedented controlled manner. This approach allows getting rid of the evaporation process and to control with accuracy the cohesion strength of the sand bed. The use of silicon oil instead of water offers the great advantage of suppressing evaporation. We conducted wind-tunnel experiments based on this approach and quantified how the aerodynamic and dynamic thresholds vary with the liquid content.

The article is organized as follows. Section 2 describes the experimental facility and the approach employed to determine both the aerodynamic and impact erosion rates from which we deduce the aerodynamic and dynamic transport thresholds. In section 3 and 4 we present the results on aerodynamic and impact erosion rates and discuss the influence of the cohesion strength of the sand bed on the respective erosion thresholds. Section 5 summarizes the outcome results and presents outlooks.

2 Experimental setup

2.1 Wind-tunnel facility

The experiments were carried out in a wind tunnel with a 6.6 m length working section and a 0.245 m×0.27 m cross-section (see Figure 1). We used as a cohesive sand bed a mixture of 0.2 mm sand and silicone oil (AR 20) with a surface tension $\Gamma = 20.6\,10^{-3}\ N/m$. The sand bed is reduced to a box with a square section of dimensions $0.15\,m$×$0.15\,m$ and a $0.02\,m$ depth. We chose a small bed sample to get a local evaluation of the erosion rate. The requirement is that the length of the sample be much smaller than the saturation length but not too small for statistical representative measurements. We will come back to the influence of the bed length on the experimental outcomes in sections 4 and 5.

The sand bed sample is placed 5.4 m downstream the entrance of the wind tunnel and its surface is at the same level as the wind-tunnel floor so that there is no discontinuity. The floor of the wind tunnel (i.e., upstream and downstream of the sand bed) was made rough by gluing sand particles of the same nature as the sand bed. The sand bed is weighed continuously during the experiment by means of a scale with a milligram accuracy. This allows to record the erosion rate in the course of time (see further details in section 3).

The air flow velocity profile upstream the sand bed was characterized with Pitot tubes displayed at 10, 15, 20, 25, 30 and 40 mm above the tunnel floor. The profile obeys a classical logarithmic law

$$U(z) = \frac{u^*}{\kappa} \ln \frac{z}{z_0}\,, \tag{6}$$

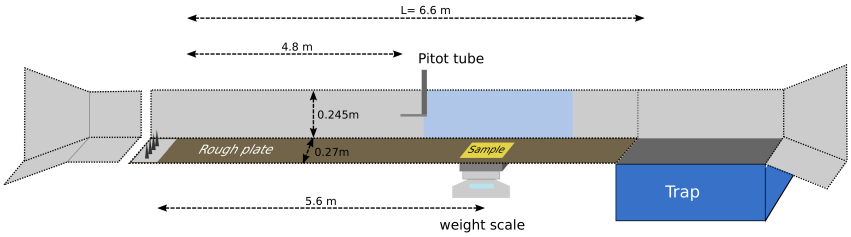

Figure 1. Wind-tunnel facility

while the friction velocity u^* follows a linear trend with the free stream velocity U_∞

$$u^* = 0.0388\, U_\infty \tag{7}$$

and the aerodynamic roughness length z_0 is roughly constant and equal to $z_0 \approx 4.10^{-6}\ m \approx D/50$.

2.2 Sand-oil mixture elaboration

Several sand-oil mixtures of about 1 *kg* were elaborated with various liquid content ranging from $w = 0.025\%$ to $w = 0.4\%$. Each mixture was prepared in a large container and homogenized manually using a metal rod. The mixture is then poured layer by layer in the dedicated box. Each layer is about 5 *mm* height and is smoothed out by a level rake before pouring the next layer. The particle volume fraction of the obtained packing slightly decreases with increasing liquid content (see Table 1). However, the decrease is relatively weak except for the two largest liquid contents ($\omega = 0.3\%$ and 0.4%). For $\omega = 0$, we obtained a volume fraction of $\phi = 0.558$ while for $\omega = 0.2\%$, we get $\phi = 0.545$.

$\omega(\%)$	0	0.025	0.05	0.075	0.1	0.2	0.3	0.4
ϕ	0.558	0.559	0.556	0.551	0.551	0.545	0.520	0.500

Table 1. Mixtures used in the experiments and corresponding volume fractions of the sand packings.

2.3 Upstream conditions

We used two different protocols to determine the static and dynamic threshold described below. For the assessment of the static threshold, the upstream air flow is free of particles and the air flow velocity is increased by successive incremental steps. A prescribed air flow velocity is set for a duration of 10 minutes and the mass of the packing is recorded in real time during the run. If the run led to a finite erosion of the sand bed, the packing is rebuilt entirely for the next run. If not, the air flow velocity is incremented using the same packing. When a packing is newly built, the first process is to raise the wind speed above the transport threshold for a short time in order to remove the unstable grains lying at the surface of the packing (McKenna-Neuman & Nickling, 1989).

For assessing the dynamic threshold, similar experiments were conducted but a given incoming particle flux at the entrance of the wind-tunnel. To do this, a hopper filled with dry sand was placed on the roof of the tunnel at 0.5 *m* downstream the entrance. The hopper was designed to feed the air flow with a constant and small incoming sand flux $Q_{in} \approx 48\, g/s$. We

used a sufficient small incoming flux which can be transported by weak winds, that is with speeds lower than the dynamic threshold obtained with a cohesionless erodible bed. The sand bed is then subject to a finite impacting flux Φ that depends both on Q_{in} and the air flow velocity. This procedure allows assessing the erosion rate by impact and to infer the dynamic transport threshold as explained in further details in Section 4.

3 Aerodynamic erosion

3.1 Temporal variation of the erosion rate

The continuous recording of the mass M of the sand bed allows determining the temporal evolution of the erosion rate during a given experiment, achieved with a prescribed wind speed. The erosion rate E is defined as

$$E = -\frac{1}{S}\frac{dM}{dt} \tag{8}$$

where S is the surface area of the sand bed. Our measurements reveal that is constant during the first stage of the erosion process. In a second stage, the erosion rate decreases with time, corresponding to the moment where the bed surface is no longer flat due to scouring effects at the downwind of the bed. The second stage occurs when the cumulative mass loss exceeds approximately $\Delta M \approx 4\ g$ (Note that a single layer of grains is a bit less than $1\,g$). In the following, we disregard the second stage of the erosion and infer the erosion rate only from measurements taken in the first stage of the erosion process. The erosion rate is thus calculated via the slope of the curve $M(t)$ in the linear regime.

3.2 Erosion rate versus Wind speed

We have measured the erosion rate as a function of the wind strength for sand beds with various liquid contents, ω ranging from 0.025% to 0.2%. For higher liquid contents (i.e., ω = 0.3 and 0.4) we were not able to reach the transport threshold which was beyond the maximum wind speed we can reach in our wind-tunnel (i.e., $U_\infty \approx 25\ m/s$ corresponding to a friction velocity $u^* \approx 1\,m/s$). The data presented in Fig. 2.a indicate that for a given liquid content, the erosion rate follows an exponential growth with the wind friction speed u^*:

$$E = A_e\ \exp\left(\frac{u^*}{u_e^*}\right), \tag{9}$$

where u_e^* is the characteristic friction velocity of the exponential growth (see Fig. 2.b).

The exponential behavior suggests that transport could be initiated at a vanishing friction velocity if one waits for an infinite time. The origin of the exponential trend is not clear to us, but could be possibly ascribed to the turbulent fluctuations of the air flow. This result then leaves us with the unresolved issue of how to determine a static threshold with a relevant criterion in the experiments. Stout and Zobeck (1996) indeed, emphasized that the determination of a threshold is dependent on the time of the measure. They also indicate that although the threshold is sensitive to the time of the measure, it remains finite. These arguments suggest that the experimental assessment of the aerodynamic threshold of transport may depend on the set-up and experimental procedure.

Here, we define the aerodynamic threshold as the erosion rate E overcomes a definite critical value E_c. We chose a critical value $E_c = 4.10^{-3}\ g/m^2 s$, that corresponds roughly to a mass loss $\Delta M \approx 5.410^{-2}\ g$ within 10 mn (which is the typical experiment duration). We selected this value because it is just above the accuracy of the weigh scale. A different choice for the critical value E_c would of course affect the assessment of the transport threshold but in the range of less than 10% variation. Using the above criterion, we determine the aerodynamic threshold for our various cohesive sand beds (see Fig. 3). We find that the static threshold friction velocity increases linearly with the liquid content:

$$u_{sw}^* = u_s^*\,(1 + a_\omega\,\omega)\ , \tag{10}$$

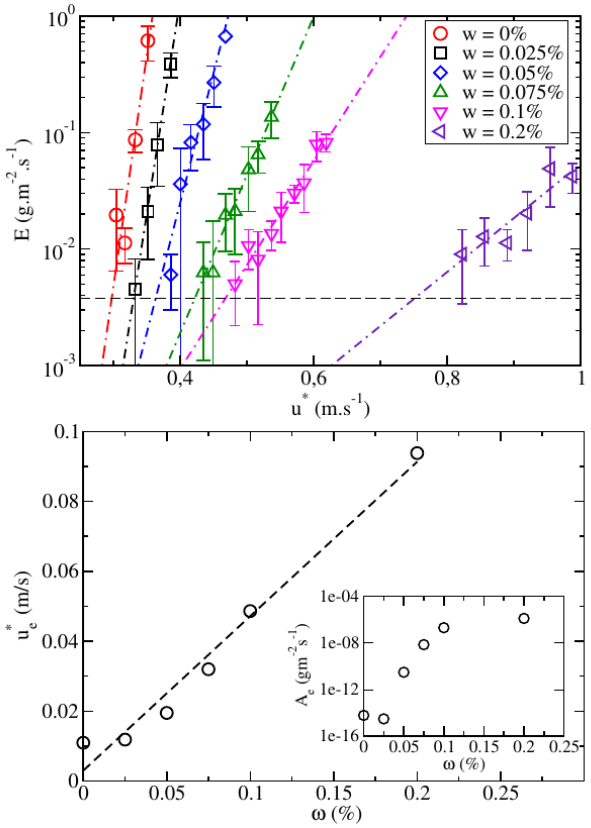

Figure 2. (a) Erosion rate E as a function of the friction speed u^* for different liquid content w. The dash-doted lines represent exponential fits to the data. The horizontal dash line stands for the critical value of the erosion rate E_c used to define the threshold friction velocity to initiate transport. (b) Characteristic friction velocity u_e^* (see Eq. 9) as a function of ω. Inset: Amplitude A_e of the exponential growth as a function ω.

with $a_\omega \approx 7 \pm 0.5$. The static threshold for cohesionless sand (i.e., $\omega = 0$) is rather large ($u_s^* = 0.3\ m/s$) in comparison with the values of the literature ($u_s^* \approx 0.21\ m/s$ (Ho et al., 2011)). This discrepancy is so important that it can not be ascribed to the uncertainty of the measurements. We strongly believe that this is due to the finite size of the sand bed. Indeed, the length of the sand bed is expected to play a significant role in the initiation of the transport since the latter is triggered by events of low probability. A long bed will thus make the occurrence of such events more likely than for a short bed. It is hard to tell what would be the relevant bed length to get size-independent results. This issue is of significant importance and would deserve a specific study which is out of the scope of this article. Besides this, our results are in line with those from Hotta et al. (1984) concerning the linear increase with ω. However, the coefficient a_ω is about 10 times greater than that found by Hotta et al. (1984) for a sand bed with similar grain size (i.e., $D = 0.2\ mm$) but mixed with water and subsequent potential evaporation phenomena. These results thus suggest that the oil modifies quantitatively the cohesion strength but not qualitatively.

Interestingly, we can take advantage of the relationship from McKenna-Neuman and Nickling (1989) (cf Eq. 4) to get an estimation of the strength of the cohesion force in terms of the cohesion number. Plugging Eq. 10 in Eq. 4 yields:

$$Co \approx \frac{a_\omega\, \omega}{3}\,(2 + a_\omega\, \omega) \tag{11}$$

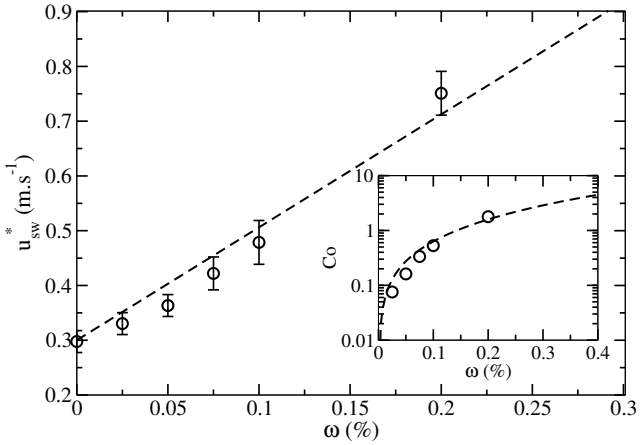

Figure 3. Static threshold u^*_{sw} as a function of the liquid content ω. The dash line corresponds to a linear fit to the data (see Eq. 10). Inset: The cohesion number Co as a function of the liquid content. The cohesion number Co is obtained from Eq. 4. The dash line corresponds to the predicted cohesion strength computed from the linear relationship between the threshold friction velocity and the liquid content: $Co = (a_\omega\,\omega/3)(2 + a_\omega\,\omega)$.

The cohesion number varies between 0.01 to 2 (see the inset of Fig. 3). The magnitude of the cohesive strength can be compared with that produced by the capillary force: $Co_{cap} = \pi D\Gamma/mgD \approx 120$ (with $D = 0.2\ mm$, $\rho_p = 2650\ kg/m^3$ and $\Gamma = 20.610^{-3}\ N/m$). The estimated cohesion strength of the investigated sand beds is thus two order of magnitude less than the capillary force, which indicates that cohesion is probably driven by very thin films adsorbed on the grains rather than liquid capillary bridges.

4 Impact erosion

4.1 Upstream mass flux

To investigate the erosion by impact, we modified the upstream condition by prescribing a small but finite incoming mass flow rate $Q_{in} = 0.48\ g/s$ at the entrance of the wind-tunnel. With this prescribed incoming flux, experiments should be operated at a friction velocity equal or greater than $0.15\ m/s$. Below this value, the air flow is not able to transport the prescribed mass flux and deposition occurs, resulting in a decreasing mass flow rate with downstream distance.

The grains released at the entrance of the wind tunnel experience a saltation motion over a rigid and rough bed and are expected to be quickly in equilibrium with the flow. Their equilibrium downstream velocity, as well as their mean saltation height and length, are governed by the strength of the flow. It is necessary to characterize the properties of the saltating grains when they impact the sand. Two important properties should be determined: the vertical flux Φ (i.e., the number of particles impacting per unit area) and the mean velocity u_p of the impacting particles. The impact erosion rate E depends on both quantities and can be expressed as

$$E = \Phi \times N_E(u_p, Co\ldots)\,, \tag{12}$$

where N_E is the average number of ejected grains per impact produced by impacting particles having a mean velocity u_p. N_E is expected to depend as well on the cohesion number Co. We should emphasize here that N_E is of course closely related to the number of ejected grains per impact determined in splash experiments (Beladjine et al., 2007) but it is different. Indeed, in splash experiments, the number of ejected grains per impact, $N_{ej}(\xi)$, is assessed for a well-

controlled impact velocity ξ. This is not the case in the present experiment where the impacting particles can exhibit a quite significant dispersion around the mean value u_p. We can infer $N_E(u_p)$ from $N_{ej}(\xi)$ if the distribution of the particle velocity is known. The calculation is done in Appendix A where a Gaussian velocity distribution is assumed.

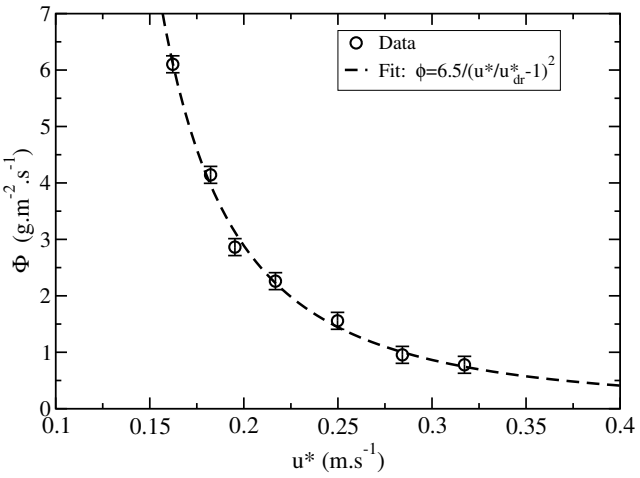

Figure 4. Impact flux Φ as a function of the shear velocity u^* for a given incoming flux $Q_{in} = 0.48\ g/s$.

The mean velocity of the impacting particles can be estimated from the measurements made by Ho (2012). He reported that the equilibrium velocity of saltating particles over a rigid bed is completely determined by the flow strength and proposed the following empirical relationship for 0.2 *mm* sand grains,

$$\frac{u_p}{\sqrt{gd}} \approx 80 \left(u^*/u^*_{reb} - 1 \right) , \tag{13}$$

where u^*_{reb} is the critical shear velocity to sustain a steady saltation motion of a single grain on a rigid and rough bed with $u^*_{reb} \approx 0.128\ m/s$. This critical friction velocity can be interpreted as the rebound threshold on a rigid bed (Pähtz et al., 2020, 2021). The relation holds as long as the flow is far from being saturated, that is, when the saltation layer is so dilute that the sand grains do not have any feed-back effect on the flow.

The impact flux Φ was directly measured by trapping the impacting grains at the location of the sand bed. To do so, we replaced the sand bed by an equivalent surface acting as a sand trap. The container used for the sand bed was filled instead with a viscous liquid (sunflower oil). Doing so, we avoid both evaporation of the liquid and ensure an efficient trapping. The flux is assessed by the same system of weighing used to determine the erosion rate. Fig. 4 presents the variation of the vertical flux Φ as a function of the shear velocity u^* for a prescribed incoming mass flux $Q_{in} = 0.48\ g/s$. As expected, the latter decreases with increasing shear velocity and the decreasing trend is well captured by

$$\Phi \propto \frac{Q_{in}}{(u^*/u^*_{reb} - 1)^2} . \tag{14}$$

This is in agreement with the findings from Ho et al. (2011). In a steady and fully developed state of transport, the impact flux is given by $\Phi = Q/l_{salt}$ where l_{salt} is the mean saltation length and Q the mass flow rate. Ho et al. (2011) showed that over a rigid and rough bed, the mean saltation length scales as $(u^*/u^*_{reb} - 1)^2$, which is fully compatible with our results on Φ.

4.2 Experimental results

As the impacting flux is varying in our experiments, the impact erosion rate E is rescaled by the impacting flux Φ and can be interpreted as the mean number of particles ejected by a single impact. The experimental data are reported in Fig. 5 where we display the rescaled erosion rate E/Φ as a function of the friction velocity for 4 different cohesion strengths. We can clearly identify a critical friction velocity u_d^* for impact erosion. We interpret this critical velocity as the dynamic transport threshold.

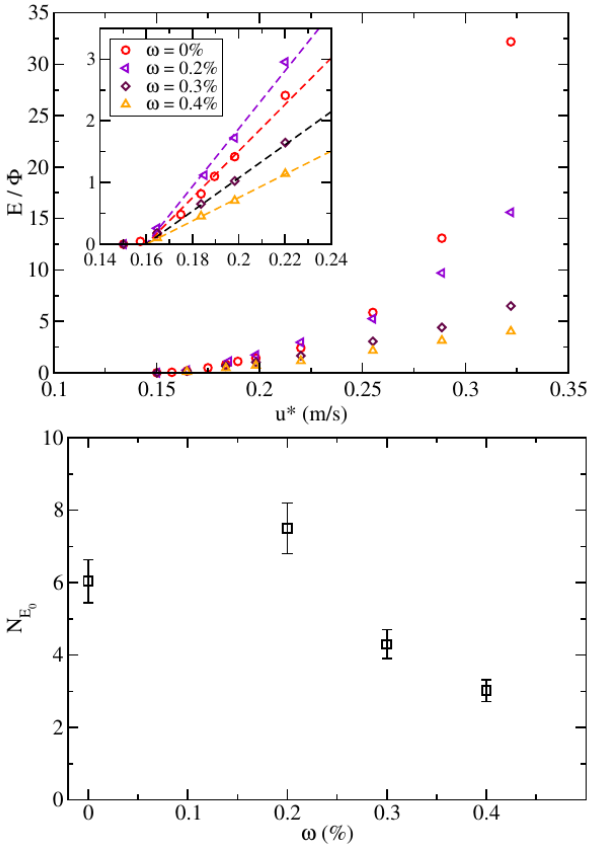

Figure 5. (a) Rescaled impact erosion rate E/Φ as a function of the friction velocity for different cohesion strengths. Inset: Magnification of the region close to the threshold, underlining the linear trends of the impact erosion rate. (b) N_{E_0} as a function of the liquid content ω (see Eq. 15).

The first salient result is that the dynamic transport threshold is insensitive to the level of cohesion of the bed: $u_d^* \approx 0.16\ m/s$. This threshold value is consistent with those found in the literature in the context of cohesionless sand beds. For example, Ho et al. (2011) reported a dynamic threshold $u_d^* \approx 0.17\ m/s$ for 0.2 *mm* cohesionless sand, consistent with our value. In contrast to what found for the aerodynamic threshold, this agreement suggests that the outcomes concerning impact erosion are not much sensitive to the size of the sand bed sample. Interestingly, the value of the dynamic threshold corresponds to a critical mean particle velocity $u_{p,0} \approx 20\sqrt{gd}$. According to Creyssels et al. (2009) and as shown in appendix A, we can infer from $u_{p,0}$ the critical impact velocity ξ_0 to trigger the erosion process: $\xi_0 \approx 2\,u_{p,0} \approx 40\sqrt{gd}$. The obtained value for ξ_0 is in agreement with that found from model collision experiments with 6 *mm* plastic beads (Beladjine et al., 2007).

The second salient result is that close to the threshold, the rescaled impact erosion rate E/Φ obeys an linear law

$$\frac{E}{\Phi} \approx N_{E_0}(\omega)\left(\frac{u^*}{u_d^*} - 1\right), \tag{15}$$

where N_{E_0} is a fitting parameter (see Fig. 5.b). Two important comments follow. Using the relationship between the mean particle velocity and the air friction velocity (cf Eq. 13), the rescaled impact erosion rate E/Φ can be expressed in terms of the mean particle velocity of the impacting grains:

$$\frac{E}{\Phi} \approx \frac{N_{E_0}(\omega)}{5}\left(\frac{u_p}{u_{p,0}} - 1\right). \tag{16}$$

To derive this relationship, we used that $u_d^*/u_{reb}^* \approx 5/4$. The critical velocity $u_{p,0}$ can be interpreted as the mean particle velocity at which the replacement capacity is equal to 1. We found that the critical mean particle velocity $u_{p,0}$ is not modified by the cohesion strength of the packing. Only, the efficiency of the impact erosion rate encoded through the quantity N_{E_0} is altered by the cohesion. N_{E_0} decreases significantly for liquid contents ω equal or greater than 0.3% (i.e., $Co \geq 3$). We can note that for $\omega = 0.2$, the coefficient N_{E_0} is a bit greater than for cohesionless beds (see Table 1). This may be probably explained by the fact that the packing fraction of the cohesive packing is slightly smaller than the cohesionless one. The bed is therefore looser and may enhance the erosion by impact.

The second important point to mention is that the linear behavior of the impact erosion rate E with the air friction velocity or mean particle velocity is observed only close to the dynamic threshold (i.e., $0.16\ m/s < u^* < 0.22\ m/s$). Far above the threshold, the increase becomes non-linear with a power-law greater than 1. Several plausible additional physical mechanisms may act in concert to increase the efficiency of the measured erosion rate at high friction velocity. An additional contribution may result from the direct aerodynamic erosion but also from a chain reaction process. Indeed, as the bed has a finite size, the ejected grains may rebound several times before leaving the bed. If the latter are sufficiently accelerated by the wind, they can trigger other ejection events as they hit the bed as in a chain reaction process. We believe that this process is responsible for the non-linear behavior of the erosion rate at high friction velocity.

5 Discussion and conclusion

With our original experimental set-up, we were able to assess the aerodynamic and impact thresholds in the context of the cohesive sand beds. Importantly, we used oil silicone instead of water to make the sand bed cohesive. This allows to get rid of the issue of water evaporation which makes difficult to control the cohesion properties of the bed in the course of time.

The first major experiment outcome is that the aerodynamic threshold friction velocity increases linearly with the liquid content, while the dynamic threshold remains unchanged with increasing cohesion strength, in the range of cohesion investigated so far (i.e., up to cohesion number $Co \approx 4.5$). We ascribe the invariance of the dynamic transport threshold with cohesion to the splash process and in particular to the fact that the critical impact velocity ξ_0 to trigger the ejection process is unaffected by cohesion in this range. A similar result was reported in numerical simulations of the impact process on cohesive granular packings by V. Ralaiarisoa et al. (2022). The numerical outcomes indicate that the critical impact velocity is unchanged as long as the cohesion number is less than 5. According to that prediction, an effect is expected to appear for liquid content ω equal or greater than 0.45%, which was not reached in our experiments. There are alternative explanations for the invariance of the dynamical threshold as proposed by Pähtz et al. (2021). They relate the dynamic threshold to the rebound threshold, which is indeed weakly dependent on the level of cohesion as reported in the numerical simulations by Comola, Gaume, et al. (2019).

The second feature is that the erosion by impact becomes less efficient for cohesion number equal or larger than 3 (N_{E_0} decreases when $Co \geq 3$) although the dynamic threshold re-

mains unchanged. According to the numerical outcomes by V. Ralaiarisoa et al. (2022), the splash process and its efficiency are not affected for cohesion number $Co \leq 5$, indicating a possible discrepancy between the experimental and numerical outcomes. However, as shown in Appendix A, the impact erosion rate E depends of course on the efficiency of the splash process but also on the nature of the velocity distribution of the impact particles. Increasing the air flow velocity may affect the velocity distribution. As an example, an increase of the vertical impact velocity fluctuation (i.e., T_y) results in the reduction of the erosion rate (see Eq.A10). We can not therefore conclude definitively about the cause of the decrease of N_{E_0} for cohesion number between 0.3 and 0.5. A decreasing efficiency of impact erosion rate should have important consequences on the equilibrium length to reach the equilibrium mass flux. In particular, this would lead to an augmentation of the equilibrium length.

The third important result is that aerodynamic erosion rate shows an exponential increase with the friction velocity both for cohesionless and cohesive beds. This raises the question of setting an appropriate criterion to define a meaningful aerodynamic threshold. To circumvent this difficulty, we used a criterion based on a critical value of the erosion rate in compliance with the weigh scale accuracy. In contrast, the impact erosion rate obeys a linear law with the friction velocity.

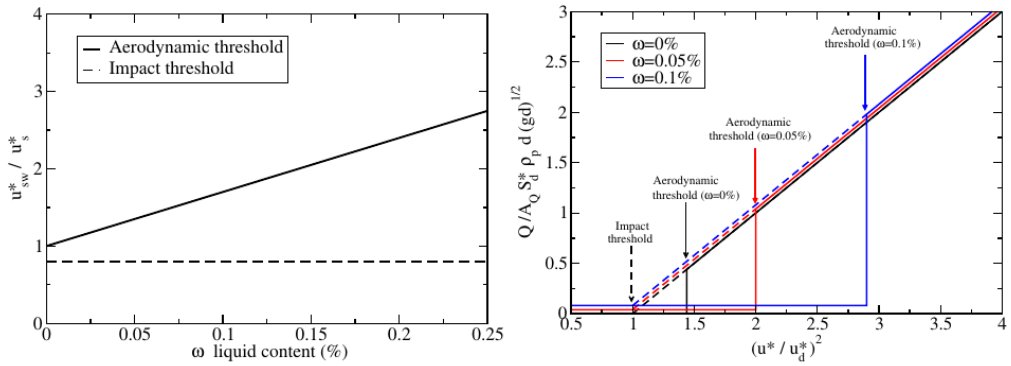

Figure 6. (a) Aerodynamic and Impact thresholds as a function of the liquid content. (b) Conjectured mass transport rate at equilibrium and bi-stable domain for various liquid content: This graph illustrates the increase of the range of the bi-stable domain (i.e., $u_d^* < u^* < u_{sw}^*$) with increasing cohesion. Here we conjectured that the mass transport law at equilibrium is unchanged for cohesive granular beds (see Eq. 5).

The most impressive effect of the cohesion is to increase the difference between the static and dynamic threshold (see Fig. 6.a). A practical consequence of this outcome is the development of strong hysteretic behaviors due to bi-stability if the wind friction velocity lies between the static and dynamic threshold. Indeed, for increasing cohesion strength, the range of the bi-stable domain strongly increases (see Fig. 6b). As a consequence, the experimental assessment of the mass flow rate in this bi-stable regime could lead to a large bias because the measurements may aggregate transport states of different nature according to the upstream boundary conditions.

An important issue to be addressed in the future is the determination of the maximum transport capacity of the wind in the context of cohesive sand beds (McKenna-Neuman & Maljaars, 1998; Davidson-Arnott et al., 2005). For cohesionless sand bed, the intensity of the saturated mass flux depends on the distance of the Shields number S^* from the dynamic threshold Shields number S_d^* multiplied by the dynamic threshold friction velocity u_d^* (see Eq. 5). As the dynamic threshold is insensitive to cohesion at least in a definite range of cohesion strength (i.e., $Co < 2$), our expectation is that the saturated flux should remain independent of the bed

cohesion as illustrated in Fig. 6.b and suggested by the numerical simulations from Comola, Gaume, et al. (2019). Experimental verifications of this conjecture are currently under investigation.

Data Availability Statement

The data set corresponding to Figures 2, 3, 4 and 5 are available as Supporting Information at "https://doi.org/10.5281/zenodo.7100605" (Besnard et al., 2022). The file ReadMe indicates how the data are displayed.

Acknowledgments

We acknowledge the support of the French Research National Agency through the project ANR-17-CE01-0014.

Appendix A Calculation of the impact erosion rate

We derive here the expression of the impact erosion rate assuming that the velocity distribution of the impact particles as well as the features of the ejection process are prescribed.

Based on the numerical simulations and experiments (Oger et al., 2005; Beladjine et al., 2007), we assume that the number of particles, including the rebound, resulting from a impact at velocity ξ is given by:

$$N(\xi) = \begin{cases} 1 + N_{ej} & \text{if } \xi > \xi_0 \\ 1 & \text{if } \xi_c \leq \xi \leq \xi_0 \\ 0 & \text{if } \xi \leq \xi_c, \end{cases} \tag{A1}$$

with

$$N_{ej}(\xi) = N_0(1 - (A - B\sin^2\theta)^2)\,(\xi/\xi_0 - 1) \tag{A2}$$

ξ_0 is the critical velocity below which there is no ejection and N_{ej} is the number of ejected grains per impact when $\xi \leq \xi_0$. θ is the impact angle measured from the horizontal and The measurements for a cohesionless granular packing give $N_0 = 13$, $A = 0.86$, $B = 0.72$, and $\xi_0 = 40\sqrt{gd}$ (Beladjine et al., 2007). This relation indicates that the number of ejected particles is the product of a function that depends only on the impact angle and a linear function of the impact velocity above a threshold value ξ_0. If the velocity of the impacting particle is less than ξ_c, the impacting particle is captured by the bed ($\xi_c \approx \sqrt{gd}$),

As done in Creyssels et al. (2009), it is reasonable to assume that the velocity of the impacting grains obeys a half-Gaussian distribution (i.e., $\xi_y < 0$):

$$f = \frac{c_0}{\pi\sqrt{T_x}\sqrt{T_y}} e^{-(\xi_x - u_p)^2/2T_x} e^{-\xi_y^2/2T_y}\,, \tag{A3}$$

where ξ_x and ξ_y are the horizontal and vertical components of the impact velocity $\vec{\xi}$ (ξ_y is negative for impacting particle), c_0 is the concentration of the impacting particle at the bed, u_p is the mean horizontal velocity of the impacting particles, $T_x = \langle \xi_x^2 \rangle$ and $T_y = \langle \xi_y^2 \rangle$.

With these assumptions, the impact erosion rate reads:

$$E = m \int_{\xi_y<0} (N-1)\xi_y f(\xi) d\xi_x d\xi_y \tag{A4}$$

Following Creyssels et al. (2009), the erosion rate can be split into two contributions: the rate of ejected grains, E_{ej}, and the rate of grains trapped by the bed, E_{loss}, which are given respectively by

$$E_{ej} = m \int_{\xi_y<0, \xi>\xi_0} f(\vec{\xi}) N_{ej}(\vec{\xi}) |\xi_y| d\vec{\xi}\,, \tag{A5}$$

$$E_{loss} = m \int_{\xi_y<0, \xi<\xi_c} f(\vec{\xi}) |\xi_y| d\vec{\xi}\,. \tag{A6}$$

The result of the integration yields (Creyssels et al., 2009):

$$E_{ej} \approx \frac{mc_0N_0}{\pi\sqrt{T_xT_y}}\frac{T_x^3}{u_p(\xi_0-u_p)^2}e^{-(\xi_0-u_p)^2/2T_x}\times\left(1-A^2+AB\sqrt{\frac{2\pi T_x}{\xi_0 u_p}}\right), \tag{A7}$$

$$E_{loss} \approx 74\frac{mc_0}{\pi\sqrt{T_xT_y}}\xi_c^3 e^{-u_p^2/(2T_x)} \ . \tag{A8}$$

The impact erosion rate vanishes when E_{ej} balances exactly E_{loss}. Assuming that $u_p \gg \sqrt{T_x}$, the balance reduces to (Creyssels et al., 2009):

$$u_p \approx \frac{\xi_0}{2} \tag{A9}$$

This means that the erosion rate vanishes when the mean particle velocity of the impacting particle equals the critical velocity $u_{p,0} \approx \xi_0/2$. The critical mean particle velocity is thus completely linked to the critical impact velocity ξ_0 to trigger the ejection process. A linear expansion around $u_{p,0}$ provides a approximate for the erosion rate which yields to first order:

$$E \approx \phi N_0\left(1-A^2+AB\sqrt{\frac{4\pi T_x}{\xi_0^2}}\right)\frac{2T_x^{3/2}e^{-\xi_0^2/8T_x}}{\pi\xi_0 T_y}\left(\frac{u_p}{u_{p,0}}-1\right) \tag{A10}$$

where $\phi = mc_0\sqrt{T_y}$ is the vertical impacting mass flux. If we take a typical value of T for saltation transport on a rigid and rough bed (Ho, 2012) ($T_x \approx T_y \approx 200\,gd$), we get: $E \approx 0.5\,\phi\,(u_p/u_{p,0}-1)$ which is of the same order of magnitude as what found in the experiments for cohesionless sand bed ($E(\omega=0) \approx \phi\,(u_p/u_{p,0}-1)$; see Eq. 16).

References

Andreotti, B., Claudin, P., Iversen, J. J., Merrison, J. P., & Rasmussen, K. R. (2021). A lower-than-expected saltation threshold at martian pressure and below. *Proceedings of the National Academy of Sciences*, *118*(5), e2012386118. doi: 10.1073/pnas.2012386118

Andreotti, B., Claudin, P., & Pouliquen, O. (2010). Measurements of the aeolian sand transport saturation length. *Geomorphology*, *123*, 343-348.

Bagnold, R. A. (1941). The physics of blown sand and desert dunes. *Methuen, New York*.

Beladjine, D., Ammi, M., Valance, A., & Oger, L. (2007). Collision process between an incident bead and a three-dimensional granular packing. *Physical Review E.*, *75*, 061305.

Belly, P. (1962). Sand movement by wind, united states army corps of engineers. *Coastal Engineering Research Center, Technical Memorandum, Washington*, *Vol I*.

Besnard, J., Dupont, P., Ould El Moctar, A., & Valance, A. (2022). Aeolian erosion thresholds for cohesive sand [data set]. *Zenodo*. doi: 10.5281/zenodo.7100605

Bisal, F., & Hsieh, J. (1966). Influence of moisture on erodibility of soil by wind. *Soil science*, *102*, 103-146.

Chepil, W. (1956). Influence of moisture on erodibility of soil by wind. *Soil science Society Proceedings*, *20*, 288-292.

Claudin, P., & Andreotti, B. (2006). A scaling law for aeolian dunes on mars, venus, earth, and for subaqueous ripples. *Earth and Planetary Science Letters*, *252*(1), 30-44.

Comola, F., Gaume, J., Kok, J. F., & Lehning, M. (2019). Cohesion-induced enhancement of aeolian saltation. *Geophysical Research Letters*, *46*(10), 5566-5574.

Comola, F., Kok, J. F., Chamecki, M., & Martin, R. L. (2019). The intermittency of wind-driven sand transport. *Geophysical Research Letters*, *46*(22), 13430-13440.

Cornelis, W. M., Gabriels, D., & Hartmann, R. (2004a). A conceptual model to predict the deflation threshold shear velocity as affected by near-surface soil water. *Soil Science Society of America Journal*, *68*(4), 1154-1161.

Cornelis, W. M., Gabriels, D., & Hartmann, R. (2004b). A conceptual model to predict the deflation threshold shear velocity as affected by near-surface soil water. *Soil Science Society of America Journal*, *68*(4), 1162-1168.

Creyssels, M., Dupont, P., Ould El Moctar, A., Valance, A., Cantat, I., Jenkins, J. T., ... Rasmussen, K. R. (2009). Saltating particles in a turbulent boundary layer : experiment and theory. *Journal of Fluid Mechanics*, *625*, 47-74.

Davidson-Arnott, R. G. D., MacQuarrie, K., & Aagaard, T. (2005). The effect of wind gusts, moisture content and fetch length on sand transport on a beach. *Geomorphology*, *68*, 115-129.

Davidson-Arnott, R. G. D., Yang, Y., Ollerhead, J., Hesp, P. A., & Walker, I. J. (2008). The effects of surface moisture on aeolian sediment transport threshold and mass flux on a beach. *Earth Surface Processes and Landforms*, *33*(1), 55-74.

Duran, O., Claudin, P., & Andreotti, A. (2011). On aeolian transport: Grain-scale interactions, dynamical mechanism and scaling laws. *Aoelian Research*, *3*, 243-270.

Han, Q., Qu, J., Zhang, K., Zu, R., Niu, Q., & Liao, K. (2009). Wind tunnel investigation of the influence of surface moisture content on the entrainment and erosion of beach sand by wind using sands from tropical humid coastal southern china. *Geomorphology*, *104*(3), 230-237.

Ho, T. D. (2012). *Experimental study of saltating particles in a turbulent boundary layer* (Unpublished doctoral dissertation). University of Rennes 1.

Ho, T. D., Valance, A., Dupont, P., & Ould El Moctar, A. (2011). Scaling laws in aeolian sand transport. *Physical Review Letters*, *106*, 094501.

Hotta, S., Kubota, S., Katori, S., & Horikawa, K. (1984). Sand transport by wind on a wet sand surface. In *Coastal engineering 1984* (p. 1265-1281).

Jenkins, J., & Valance, A. (2014). Periodic trajectories in aeolian sand transport. *Physics of Fluid*, *26*, 073301.

Kok, J., & Rennó, N. (2009). A comprehensive numerical model of steady state saltation. *Journal of Geophysical Research. Atmospheres*, *114, D17204*.

Louge, M. Y., Valance, A., elMoctar, A. O., Xu, J., Hay, A. G., & Richer, R. (2013). Temperature and humidity within a mobile barchan sand dune, implications for microbial survival. *Journal of Geophysical Research: Earth Surface*, *118*(4), 2392-2405. doi: https://doi.org/10.1002/2013JF002839

Louge, M. Y., Valance, A., Mint Babah, H., Moreau-Trouv, J.-C., Ould el Moctar, A., Dupont, P., & Ould Ahmedou, D. (2010). Seepage-induced penetration of water vapor and dust beneath ripples and dunes. *Journal of Geophysical Research: Earth Surface*, *115*(F2). doi: https://doi.org/10.1029/2009JF001385

Louge, M. Y., Valance, A., Xu, J., Ould el Moctar, A., & Chasle, P. (2022). Water vapor transport across an arid sand surfacenon-linear thermal coupling, wind-driven pore advection, subsurface waves, and exchange with the atmospheric boundary layer. *Journal of Geophysical Research: Earth Surface*, *127*(4), e2021JF006490.

Martin, R. L., & Kok, J. F. (2018). Distinct thresholds for the initiation and cessation of aeolian saltation from field measurements. *Journal of Geophysical Research: Earth Surface*, *123*(7), 1546-1565.

McKenna-Neuman, C., & Maljaars, M. S. (1998). A wind tunnel study of the influence of pore water on aeolian sediment transport. *Journal of Arid Environments*, *39*, 403-419.

McKenna-Neuman, C., & Nickling, W. G. (1989). A theoritical and wind tunnel investigation of the effect of capillary water on the entrainment of sediment by wind. *Canadian Journal of Soil Science*, *69*(1), 79-96.

Namikas, S. L., & Sherman, D. J. (1995). A review of the effects of surface moisture content on aeolian sand transport. In V. P. Tchakerian (Ed.), *Desert aeolian processes* (pp. 269–293). Dordrecht: Springer Netherlands.

Oger, L., Ammi, M., Valance, A., & Beladjine, D. (2005). Discrete element method to study the collision of one rapid sphere on 2d and 3d packings. *The European Physical Journal E*, *17*, 467-476.

Pähtz, T., Clark, A. H., Valyrakis, M., & Durn, O. (2020). The physics of sediment transport initiation, cessation, and entrainment across aeolian and fluvial environments. *Reviews of Geophysics*, *58*(1), e2019RG000679.

Pähtz, T., Liu, Y., Xia, Y., Hu, P., He, Z., & Tholen, K. (2021). Unified model of sediment

transport threshold and rate across weak and intense subaqueous bedload, windblown sand, and windblown snow. *Journal of Geophysical Research: Earth Surface*, *126*(4), e2020JF005859.

Pähtz, T., Valyrakis, M., Zhao, X.-H., & Li, Z.-S. (2018). The critical role of the boundary layer thickness for the initiation of aeolian sediment transport. *Geosciences*, *8*(9).

Ralaiarisoa, J.-L., Besnard, J.-B., Furieri, B., Dupont, P., Ould El Moctar, A., Naaim-Bouvet, F., & Valance, A. (2020, May). Transition from saltation to collisional regime in windblown sand. *Phys. Rev. Lett.*, *124*, 198501.

Ralaiarisoa, V., Dupont, P., Moctar, A. O. E., Naaim-Bouvet, F., Oger, L., & Valance, A. (2022, May). Particle impact on a cohesive granular media. *Phys. Rev. E*, *105*, 054902. doi: 10.1103/PhysRevE.105.054902

Ralaiarisoa, V. J.-L. (2020). *Influence de la cohésion sur le transport éolien de particules : application au sable humide et à la neige* (Unpublished doctoral dissertation). Université Rennes 1.

Selmani, H., Valance, A., Ould El Moctar, A., Dupont, P., & Zegadi, R. (2018). Aeolian sand transport in out-of-equilibrium regimes. *Geophysical Research Letters*, *45*(4), 1838-1844.

Shao, Y., & Lu, H. (2000). A simple expression for wind erosion threshold friction velocity. *Journal of Geophysical Research: Atmospheres*, *105*(D17), 22437-22443. doi: https://doi.org/10.1029/2000JD900304

Stout, J. E., & Zobeck, T. M. (1996). The wolfforth field experiment: A wind erosion study. *Soil Science*, *161 (9)*, 616-632.

Valance, A., Rasmussen, K. R., Ould El Moctar, A., & Dupont, P. (2015). The physics of aeolian sand transport. *Comptes Rendus Physique*, *16*(1), 105-117.